



Linking 3D Soil Structure and Plant-Microbe-Soil Carbon Transfer in the Rhizosphere

Alix Vidal^{1*}, Juliane Hirte², S. Franz Bender³, Jochen Mayer², Andreas Gättinger^{4,5}, Carmen Höschen¹, Sebastian Schädler⁶, Toufiq M. Iqbal⁷ and Carsten W. Mueller¹

¹ Lehrstuhl für Bodenkunde, Technische Universität München, Munich, Germany, ² Plant-Soil Interaction Group, Division, Agroecology and Environment, Agroscope, Zurich, Switzerland, ³ Department of Land, Air and Water Resources, University of California, Davis, Davis, CA, United States, ⁴ Departement für Bodenwissenschaften, FIBL, Frick, Switzerland, ⁵ Organic Farming, Justus-Liebig-Universität Giessen, Giessen, Germany, ⁶ Global Applications Support Crossbeam, Carl Zeiss Microscopy GmbH, ZEISS Group, Oberkochen, Germany, ⁷ Department of Agronomy and Agricultural Extension, University of Rajshahi, Rajshahi, Bangladesh

OPEN ACCESS

Edited by:

Maria Luz Cayuela,
Centro de Edafología y Biología
Aplicada del Segura (CSIC), Spain

Reviewed by:

Eoin L. Brodie,
Lawrence Berkeley National
Laboratory (LBNL), United States
Lukas Van Zwieten,
New South Wales Department of
Primary Industries, Australia

*Correspondence:

Alix Vidal
alix.vidal@wzw.tum.de

Specialty section:

This article was submitted to
Soil Processes,
a section of the journal
Frontiers in Environmental Science

Received: 17 November 2017

Accepted: 26 January 2018

Published: 09 February 2018

Citation:

Vidal A, Hirte J, Bender SF, Mayer J,
Gättinger A, Höschen C, Schädler S,
Iqbal TM and Mueller CW (2018)
Linking 3D Soil Structure and
Plant-Microbe-Soil Carbon Transfer in
the Rhizosphere.
Front. Environ. Sci. 6:9.
doi: 10.3389/fenvs.2018.00009

Plant roots are major transmitters of atmospheric carbon into soil. The rhizosphere, the soil volume around living roots influenced by root activities, represents hotspots for organic carbon (OC) inputs, microbial activity, and carbon turnover. Rhizosphere processes remain poorly understood and the observation of key mechanisms for carbon transfer and protection in intact rhizosphere microenvironments are challenging. We deciphered the fate of photosynthesis-derived OC in intact wheat rhizosphere, combining stable isotope labeling at field scale with high-resolution 3D-imaging. We used nano-scale secondary ion mass spectrometry and focus ion beam-scanning electron microscopy to generate insights into rhizosphere processes at nanometer scale. In immature wheat roots, the carbon circulated through the apoplastic pathway, via cell walls, from the stele to the cortex. The carbon was transferred to substantial microbial communities, mainly represented by bacteria surrounding peripheral root cells. Iron oxides formed bridges between roots and bigger mineral particles, such as quartz, and surrounded bacteria in microaggregates close to the root surface. Some microaggregates were also intimately associated with the fungal hyphae surface. Based on these results, we propose a conceptual model depicting the fate of carbon at biogeochemical interfaces in the rhizosphere, at the forefront of growing roots. We observed complex interplays between vectors (roots, fungi, bacteria), transferring plant-derived OC into root-free soil and stabilizing agents (iron oxides, root and microorganism products), potentially protecting plant-derived OC within microaggregates in the rhizosphere.

Keywords: rhizosphere, microorganisms, iron oxides, organo-mineral associations, NanoSIMS, FIB-SEM, undisturbed samples, ¹³C enrichment

INTRODUCTION

Soils harbor a huge fraction of the global terrestrial carbon (C) pool. While belowground C transfer by plants represents a major pathway of atmospheric C into the soil, soils also represent a major source of atmospheric C. Understanding the complex interactions that govern C storage in and release from soils is a major challenge to develop strategies to mitigate climate change (Lal, 2004).

Soils are composed of a wide diversity of organic and mineral compounds, forming a complex mosaic of microenvironments (Ranjard and Richaume, 2001). The volume of soil directly affected by living roots, i.e., the rhizosphere, represents an important hotspot for microbial activity, organic carbon (OC) inputs, and C turnover in soils (Hinsinger et al., 2009; Philippot et al., 2013; Finzi et al., 2015). Root products (mucilage, exudates, cell fragments) and dead roots, represent a major source of OC in soils (Rasse et al., 2005; Bardgett et al., 2014). Around 30% of the photosynthetically fixed C is transferred below ground, but this proportion can vary widely depending on environmental conditions, plant species, and the plant growing stage (Kuzyakov and Domanski, 2000). While half of the C transferred below ground is allocated to the root biomass, around one-third is respired in the rhizosphere (Jones et al., 2009), in equal proportions by roots and microorganisms (Kuzyakov and Larionova, 2005). Finally, more than 10% of the C transported below ground is allocated to soil microorganisms and soil organic matter (Jones et al., 2009; Kaiser et al., 2015). Alive or dead, microorganisms inhabiting the rhizosphere represent a major sink for plant-derived C and foster the development of soil microstructures (Liang and Balser, 2011; Kallenbach et al., 2016; Lehmann et al., 2017). These microorganisms include arbuscular mycorrhizal (AM) fungi, soil fungi that form symbiotic associations with the majority of land plants, including wheat (Van der Heijden et al., 1998; Dickie et al., 2013). These fungi can receive up to 20% of a plant's photosynthetic C intake in return for delivery of nutrients to the plant (Jakobsen and Rosendahl, 1990). Specific surface binding properties of organic soil components (roots, plant-derived compounds, and microorganisms) together with adsorption capacities of soil minerals are drivers of the formation of complex organo-mineral assemblages as microaggregates (Baldock and Skjemstad, 2000; Bronick and Lal, 2005). The association of OC in complex microaggregate structures stabilizes C against degradation and reduces its turnover in soil, hence representing a pathway of C sequestration (Kögel-Knabner and Amelung, 2014). Rhizosphere processes have a determinant impact on the global soil C pool that is still not fully understood (Schmidt et al., 2011; Pett-Ridge and Firestone, 2017). Enhancing rhizosphere processes, such as C transfer from roots to microorganisms and soil, can increase soil C storage (White et al., 2013; Lange et al., 2015), one of the challenges of the Twenty-first century to mitigate climate change (Lal, 2004; Lehmann, 2007).

The complexity of biogeochemical processes occurring in the rhizosphere requires observations at process-relevant scales, i.e., at the interface of root cells, microorganisms, and soil (Hallett et al., 2013; Oburger and Schmidt, 2016). The microscopic observation of intact soil structures as embedded thin sections has been applied since the 1930s (Kubiena, 1938; Alexander and Jackson, 1954) and has enabled the observation of the rhizosphere at the scale of organism interactions (Martin and Foster, 1985). Despite the descriptive quality of such imaging approaches, the absence of techniques to trace specific elements and isotopes hampered the direct *in situ* study of C allocation at biogeochemical interfaces in the rhizosphere. Since then, strong efforts have been made to observe undisturbed

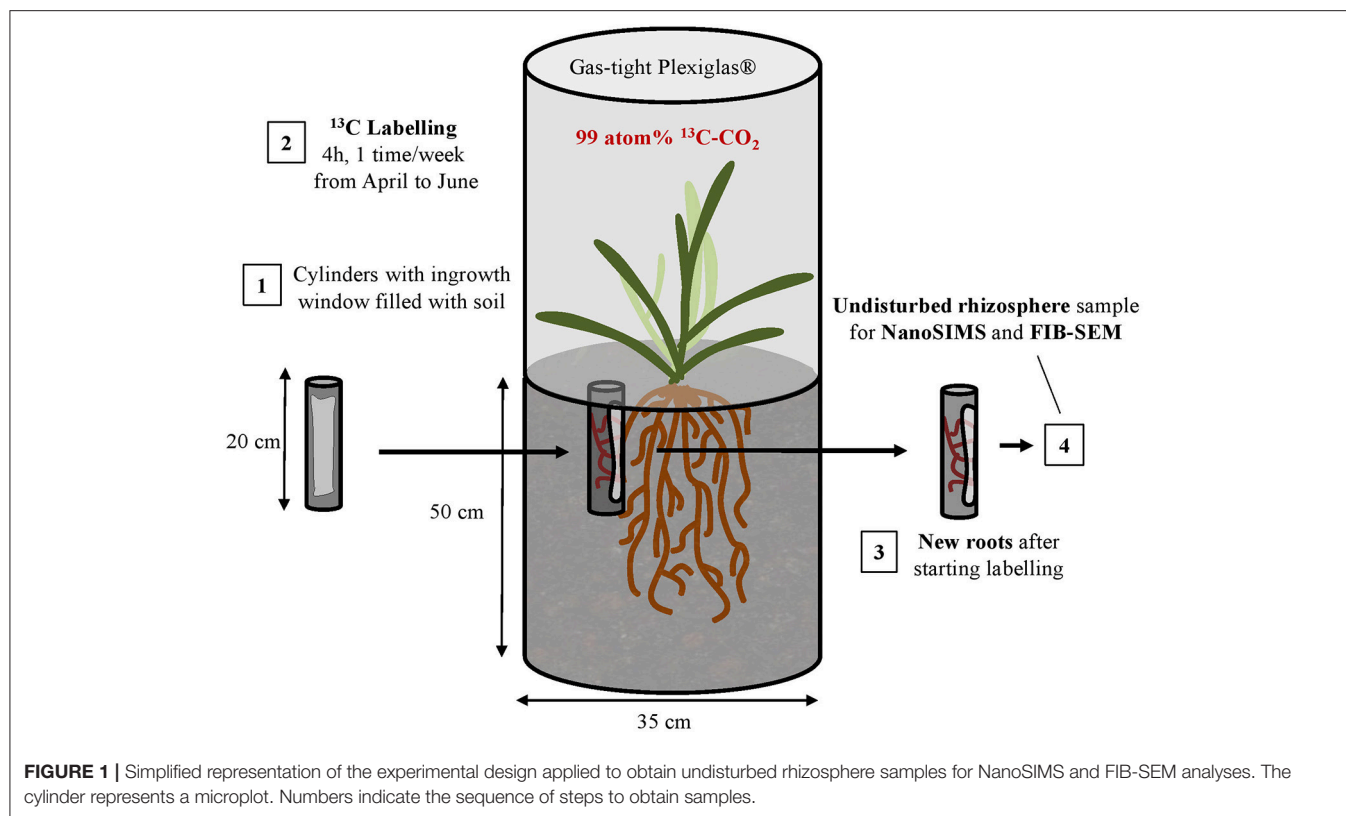
soil-root-microorganism assemblages at the microscale under controlled laboratory conditions, in some cases using ^{13}C and ^{15}N tracers (Nunan et al., 2001; Li et al., 2003; Castorena et al., 2016; Vidal et al., 2016). In the present study, we collected undisturbed rhizosphere samples in an agricultural field and considered *in situ* interactions of plants, microorganisms, and soil mineral particles at the microscale.

We qualitatively explored the pathway of photosynthetically fixed C from roots to microorganisms and soil, as well as how roots determine the structural and compositional 3D architecture of the rhizosphere at nanometer resolution. To meet this objective, we combined 2D elemental and isotopic information (nano-scale secondary ion mass spectrometry-NanoSIMS) with 3D structural information (Focused ion beam-scanning electron microscopy-FIB-SEM) highlighting biogeochemical interfaces and processes in the rhizosphere. We expected the highest enrichment in the close vicinity of roots, as well as a transfer of plant-derived C to microorganisms surrounding roots and forming intimate associations with minerals.

MATERIALS AND METHODS

In Situ ^{13}C -Labeling and Sampling

Samples were collected in 2015 on winter wheat (*Triticum aestivum*, var. Wiwa) plots of the Swiss long-term field trial "DOK" (Therwil, CH) (Mayer et al., 2015). Two microplots (stainless steel tubes, 0.35 m diameter, 0.55 m length) were inserted into the soil to 0.5 m depth to segregate wheat sub-populations (approximately 50 plants in two rows) from surrounding field populations below ground. The first microplot corresponded to a full-fertilized bio-organic management system (i.e., in compliance with the subsidiary scheme "Bio Suisse"). The second microplot corresponded to a full-fertilized conventional management system (i.e., in compliance with the subsidiary scheme "Proof of Ecological Performance"). The wheat was fertilized according to Swiss standards for the respective managements (Flisch et al., 2009). The present study did not aim at comparing organic and conventional treatments but at depicting rhizosphere processes through qualitative microscale observations. Thus, the samples collected from these two microplots were not separated by treatments for NanoSIMS analyses. In order to keep labeled plants as undisturbed as possible, the use of multiple-pulse labeling was chosen instead of a more invasive method (Kuzyakov and Domanski, 2000). From advanced tillering to maturity (beginning of April to end of June according to Zadoks et al., 1974), the headspace over each microplot was enclosed with a gas-tight Plexiglas[®] hood once per week and plants were exposed to 99 atom-% ^{13}C -CO₂ (Figure 1). Before the labeling campaign, the necessary amount of label, the number of pulse events during the vegetation period, and the duration of each pulse event were calculated. For this purpose, three parameters were considered: the strength of the label (99%), the daily assimilation rate of wheat, and the targeted bulk soil enrichment. The gas was injected in repeated pulses during 4 h between late morning and early afternoon while the CO₂ concentration was regularly tracked using a portable LI-COR (LI820, re-calibrated for ^{13}C -sensitivity) and allowed to



fluctuate between 150 and 800 ppm. Closed ventilation by PC fans and cooling with 4 kg ice packs ensured similar climatic conditions inside and outside the labeling hoods. The microplot plants received approximately 9.5 g ¹³C over the entire labeling period. Considering the qualitative microscale approach of the present study, we did not include a bare fallow control to account for the autotrophic CO₂ fixation. Indeed, we focused on rhizosphere processes and assumed autotrophic microorganisms to be negligible compared to heterotrophic ones (Kuz'yakov and Larionova, 2005). For minimal destruction of microplots by the root and soil sampling before plant maturity, one root-ingrowth cylinder (PVC tubes, 30 mm diameter, 200 mm length) was inserted into the topsoil of each microplot (cylinder 1 and 2, for the organic and conventional treatments, respectively). Cylinders had an ingrowth window of 150*30 mm on one side and were covered with a 1 mm mesh on openings. Sieved and homogenized topsoil was filled into the cylinders and re-compacted to a density of 1.3 g.cm⁻³, which was estimated from the cylinder volume and the fresh soil mass. At the beginning of the labeling period, one hole per microplot was drilled in 20–30 mm distance from the wheat rows by means of a gouge auger (30 mm diameter; Eijkelkamp, Netherlands). The two ingrowth cylinders were gently pushed inside the holes so that the bottom and side walls were in close contact with the surrounding soil and the ingrowth windows faced wheat rows. Only new wheat roots that grew after the beginning of the labeling period could thereby enter ingrowth cylinders. Plants were labeled 10 times with the last labeling being conducted 3 days before sampling. At anthesis (Zadoks' scale 69;

Zadoks et al., 1974, mid-June), the cylinders were removed from the soil, transported to the laboratory, and immediately processed or deep-frozen for further analyses.

Sample Processing

The two ingrowth cylinders were opened at the top and bottom and the complete soil core within the cylinder was removed. Soil was carefully broken by hand into several pieces. Larger soil aggregates including root fragments (approximately 1 cm⁻³) were sampled. Two samples from each cylinder, i.e., four samples in total, were chemically fixed using Karnovsky fixative (Morris, 1965) and dehydrated in graded acetone series and embedded in araldite resin (Araldite 502) until complete polymerization, according to the method described by Mueller et al. (2012). Samples were cut and polished to obtain intact rhizosphere cross sections. In order to analyze the fine soil fraction containing microaggregates and fungal hyphae, a fungal hypha was extracted from cylinder 1, which showed a higher percentage of hyphal root colonization (Table 1). This sample was prepared on a silica wafer according to Mueller et al. (2012). Briefly, 1 mg of dried soil from the chemically fixed and dried rhizosphere was dispersed in 10 mL of analytical water ACS. A 100 µL drop was deposited on a silica wafer and dried overnight.

The remaining soil from cylinders was separated from roots and other organic materials by 0.5 mm wet-sieving, oven-dried at 80°C and analyzed for total C and ¹³C abundance using an elemental analyzer coupled with an isotope ratio mass spectrometer (EA 1110; Carlo Erba; coupled with Delta

TABLE 1 | General characteristics of soil and colonization with arbuscular mycorrhizal fungi of roots extracted from the two cylinders, considered as replicated in the present study and used for the NanoSIMS and FIB-SEM analyses.

	Cylinder 1	Cylinder 2
SOIL CHARACTERISTICS		
Soil texture (% sand-silt-clay)	12-72-16	12-72-16
SOC (%)	1.34	1.23
$\delta^{13}\text{C}$ (‰)	−18.1	−22.7
$\delta^{13}\text{C}$ excess (‰)	9.3	4.4
ROOT LENGTH COLONIZED BY ARBUSCULAR MYCORRHIZAL FUNGI		
Hyphae (%)	63	30
Vesicles (%)	2	1
Arbuscles (%)	4	8

S; Thermo Finnigan). The root colonization by AM fungi was assessed by microscopy using a modified line-intersection method for 100 intersections after clearing and staining with an ink-vinegar mixture as described by Wagg et al. (2011). The general characteristics of the soil are presented in **Table 1** for the two cylinders, as well as the percentage of root length colonized by AM fungal hyphae, vesicles, and arbuscles.

NanoSIMS Analyses

We analyzed intact rhizosphere sections (four transversal and longitudinal sections) and a rhizosphere derived fungal hypha with NanoSIMS. At first, the scanning electron microscope (SEM in backscatter mode; JEOL JSM 5900LV, Garching, Germany) was used to identify areas for subsequent NanoSIMS analyses. Areas of interest corresponded to intact rhizosphere area containing root cells, microorganisms, and soil minerals/microaggregates. The sample surface was sputtered by a Cs^+ beam to obtain $30 \times 30 \mu\text{m}^2$ images (acquired using a NanoSIMS 50L Cameca, Germany) at 256×256 pixels. Secondary ion images of ^{12}C , ^{13}C , ^{16}O , $^{12}\text{C}^{14}\text{N}$, and $^{56}\text{Fe}^{16}\text{O}$ were obtained and 20 planes were accumulated for each final image, with a dwell time of $1 \text{ ms} \cdot \text{pixel}^{-1}$. Measurements on the sample dispersed on the silica wafer were realized in the same manner, recording 22 planes. Higher resolution images were obtained acquiring $40 \times 40 \mu\text{m}^2$ images at 512×512 pixels for ^{12}C , ^{13}C , $^{12}\text{C}^{14}\text{N}$, and ^{16}O secondary ions. Measurements were processed using the ImageJ software (Abramoff et al., 2004). OpenMIMS and MosaicJ plugins (Thévenaz and Unser, 2007) were used to display images and create mosaics, respectively. For RGB mosaic images, images were first uploaded individually, composite RGB images were created ($^{56}\text{Fe}^{16}\text{O}$ in red, $^{12}\text{C}^{14}\text{N}$ in green, ^{16}O in blue) and adjusted to remove the resin contribution using the color adjustment. Images were then uploaded in the MosaicJ plugin for mosaic creation. Mosaics including 3–32 NanoSIMS measurements were created. The $^{13}\text{C}:^{12}\text{C}$ ratio images were generated to follow the distribution of ^{13}C enrichment. The enrichment was estimated by comparing $^{13}\text{C}:^{12}\text{C}$ ratio values to the approximate soil natural abundance (0.011). For $^{13}\text{C}:^{12}\text{C}$ ratio mosaic images, images were first uploaded individually to obtain the $^{13}\text{C}:^{12}\text{C}$ ratio distribution and uploaded in the MosaicJ plugin for the mosaic creation. The interactive regions of interest (ROIs)

definition tool of Look@NanoSIMS program (Polerecky et al., 2012) was used to draw ROIs on selected $^{12}\text{C}^{14}\text{N}$ images, in order to obtain their isotopic composition. ROIs were drawn either by using the threshold function according to $^{12}\text{C}^{14}\text{N}$ counts (microbes and hyphae), the freehand drawing option (plant cell walls) or by drawing ellipses (resin spots). The resin, which presented a $^{13}\text{C}:^{12}\text{C}$ ratio equal to the soil natural abundance was considered as natural background.

FIB-SEM Analyses

FIB-SEM imaging was performed using a Zeiss Crossbeam 550 L microscope with a primary beam operated at a landing energy of 1.8 keV. Backscattered electrons were recorded at an energy-selective backscattered electron detector with the grid voltage set to 1,000 V. The Carl Zeiss ATLAS 5 package was used for the identification of the adequate sample position by precise spatial correlation of sample stage coordinates to the previously acquired NanoSIMS analysis, and for the control of the FIB-SEM acquisition. Images were collected at $15 \mu\text{s}$ dwell time, at 10 nm pixel resolution, and at slice intervals of 10 nm. EDS maps were collected at 40 nm pixel resolution at a Z interval of 160 nm.

For the FIB sample preparation, first a $1.5 \mu\text{m}$ thick protective platinum layer was deposited on the surface of the sample's volume of interest using a 3 nA FIB beam current. The characteristic ATLAS 3D tracking marks, which are used to dynamically correct for drifts of the sample with respect to the SEM beam in x- and y-directions, and for drifts of the sample with respect to the FIB milling in z-direction, were milled into this platinum layer with a 50 pA FIB beam, filled in with a layer of C (100 pA FIB beam current) and then covered with a $1 \mu\text{m}$ thick C pad (3 nA FIB beam current). The cross-section in front of the volume of interest was opened using a 30 nA FIB beam current and then polished using a 7 nA FIB beam current.

During the collection of the imaging dataset, the FIB (3 nA beam current) and the SEM (1.8 kV, 1.0 nA) were operated simultaneously. FIB-SEM imaging was paused and the SEM ramped to analytical conditions (6 kV, 2 nA) at z intervals of 160 nm for the acquisition of EDS maps.

The 3D data set was created from the datasets using ORS Dragonfly software. Images were not aligned after the acquisition because the quality of the alignment achieved during the acquisition of the dataset was considered sufficient. The direction of image acquisition for both the FIB-SEM dataset and EDS maps is perpendicular to that for the NanoSIMS analysis and 2D surface imaging. To highlight the volumes of interest without additional segmentation steps, window levels of the images were adjusted and saturated black values made transparent in the volume view.

Statistical Analyses

The R software, version $\times 64$ 3.3.2 (R Core Team, 2017), was used for boxplot representations of ROI $^{13}\text{C}:^{12}\text{C}$ ratio values of NanoSIMS images and statistical analyses. The application of Shapiro–Wilk test revealed that data were not normally distributed. Thus, the non-parametric Kruskal–Wallis test was performed, followed by multiple pairwise comparisons with Dunn test. Statistical significance was set as $\alpha = 0.05$ for all tests.

RESULTS

Arrangement of Organic and Mineral Structures in Roots and Rhizosphere

We analyzed an immature wheat root close to the root tip (Figures 2, 3, and Supplementary Figure 1) as this is the location of highest activity in terms of mucilage production and effects on soil structure due to pressure of the growing roots. The root tip has a stele diameter of less than 100 μm and no identifiable phloem and xylem cells. The cortex cells, located

at the periphery of the root and in direct contact with the soil particles, present a marked deformation (Figure 2). This phenomenon is also observed on a longitudinal section of another root (Supplementary Figure 2).

Organic structures surrounding the root (Figures 2, 3A) are mainly represented by unicellular microorganisms (bacteria or archaea) and particulate organic matter (POM). We were able to detect the round shape of microorganisms with an approximate diameter of 1 μm and high nitrogen content reflected by the $^{12}\text{C}^{14}\text{N}$ clearly indicating its microbial origin

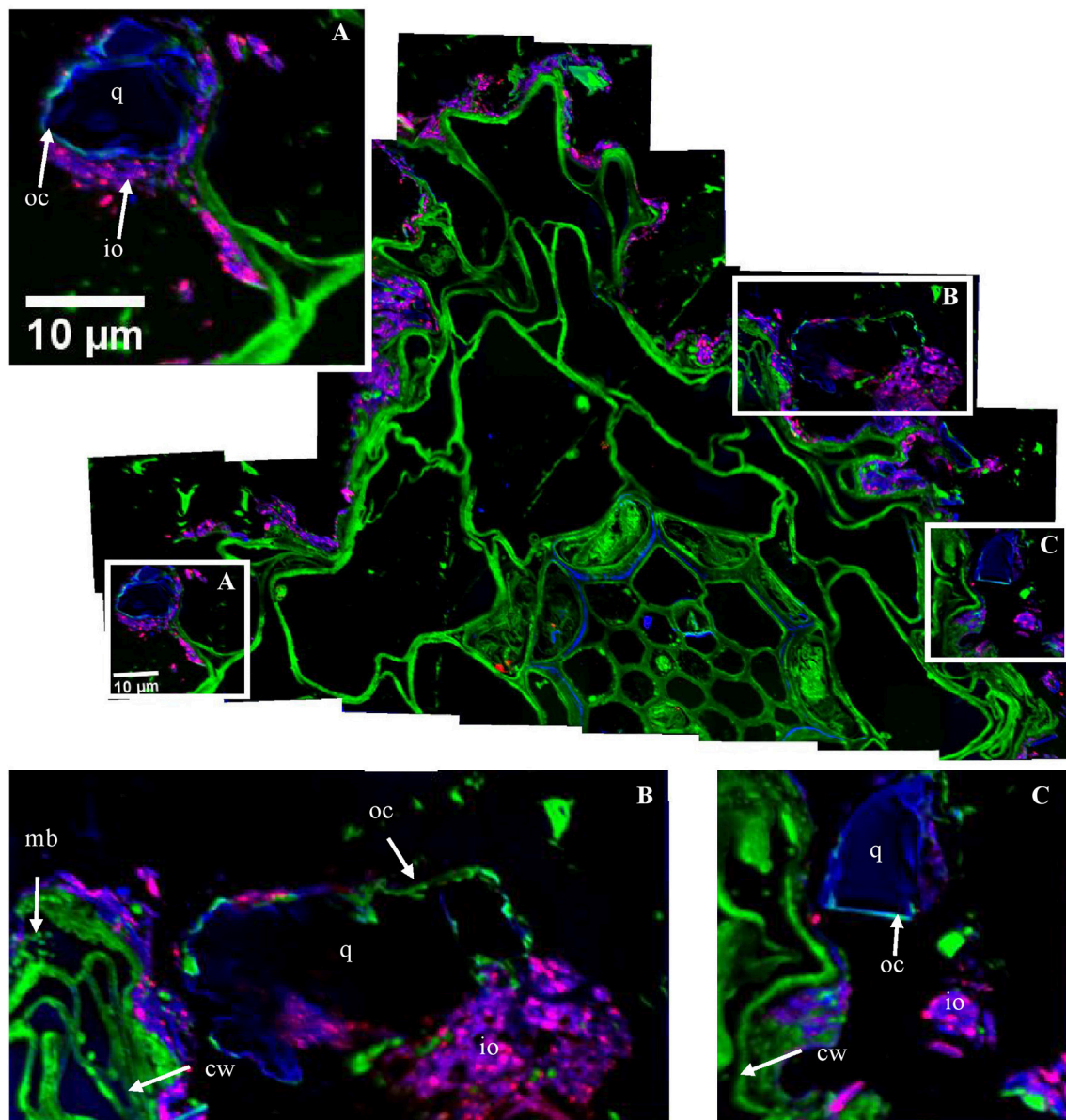


FIGURE 2 | Organo-mineral associations surrounding the root cells. Mosaic of NanoSIMS composite images of the area indicated in Supplementary Figure 1A; with $^{12}\text{C}^{14}\text{N}$ in green, ^{16}O in blue, $^{56}\text{Fe}^{16}\text{O}$ in red. The mosaic was built up from 32 NanoSIMS measurements (one image $-30 \times 30 \mu\text{m}$, 256×256 pixels, 20 planes, $1 \text{ ms} \cdot \text{pixel}^{-1}$). (A–C) Illustrate the intimate association between large mineral particles ($>10 \mu\text{m}$) (i.e., q, quartz grain); io, iron oxides; cw, plant cell walls; mb, microorganisms; and oc, organic coating. The black area represents the resin. White squares correspond to the areas used to obtain the boxplot in Figure 8.

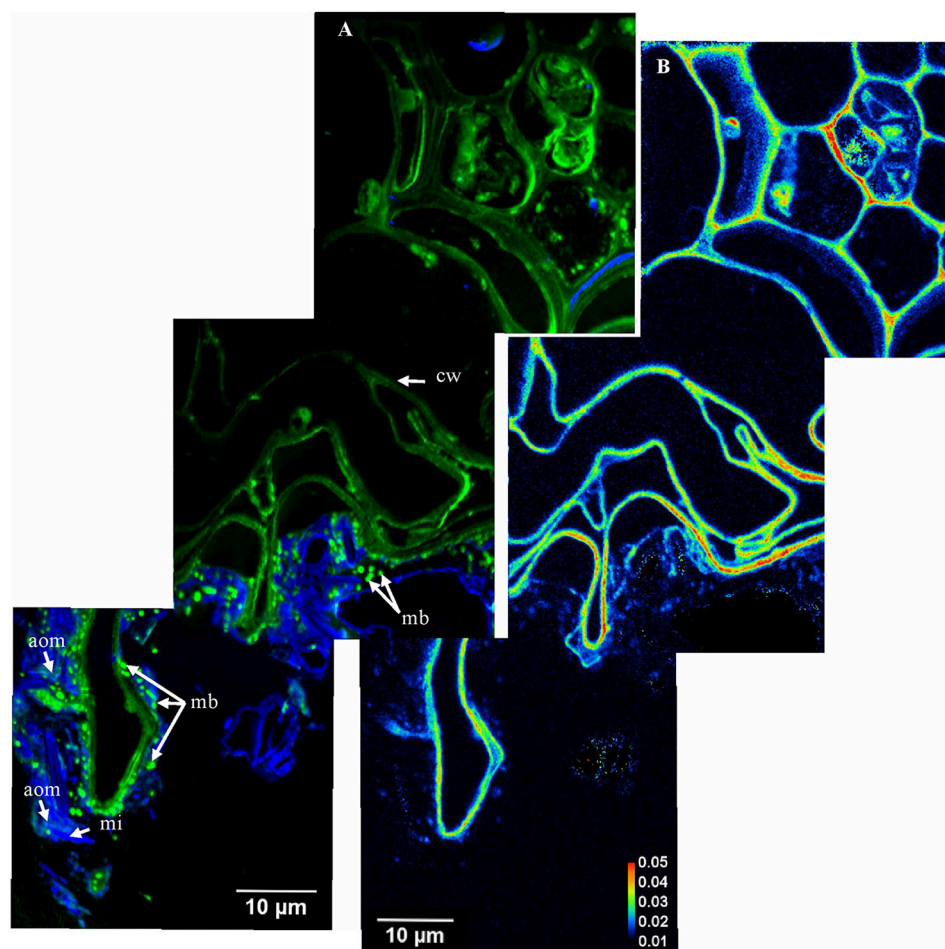


FIGURE 3 | From stele to cortex and rhizosphere—carbon transfer and organo-mineral associations. **(A)** Mosaic of NanoSIMS composite images of the area indicated in Supplementary Figure 1B; with $^{12}\text{C}^{14}\text{N}$ in green and ^{16}O in blue; aom, amorphous organic matter; cw, plant cell walls; mb, microorganisms; mi, mineral particle. The mosaic was created from 3 NanoSIMS images (one image- $40 \times 40 \mu\text{m}$, 512×512 pixels, 20 planes, $1 \text{ ms} \cdot \text{pixel}^{-1}$); **(B)** The $^{13}\text{C}:^{12}\text{C}$ ratio of the same area presented in **(A)**.

(Figure 3A). The microorganisms are mainly concentrated at the close surrounding of peripheral root cells and/or in direct contact with root cell walls (Figures 3A, 4D). From some micrometer distance to the rhizoplane, microorganisms, as well as laces of N rich POM, are identified in soil microaggregates (Figures 2, 5B). These microorganisms appear as separated cells (Figure 2) or forming microbial cell assemblages (Figure 5B) at the surrounding of roots or within soil aggregates. By using FIB-SEM we were able to demonstrate the direct association of microbial cells with clay sized soil minerals forming microaggregate precursors directly at the rhizoplane (Figure 4C). Microbial cells forming the microbial assemblage are directly bound to the root cell surface on one side and enclosed within a dense layer of mineral soil constituents.

We also extracted a fungal hypha from the rhizosphere soil to study the direct effect of fungi on microaggregate assemblages in the rhizosphere (Figure 6). Microaggregates (high ^{16}O and $^{56}\text{Fe}^{16}\text{O}$ signals) are directly attached to the hyphal surface.

Inorganic structures are represented both by larger mineral particles ($>5 \mu\text{m}$), with high ^{16}O content (Figures 2A–C, 4E, and Supplementary Figure 3C), assignable to quartz grains and iron oxides, with high $^{56}\text{Fe}^{16}\text{O}$ content (Figure 2). Clay sized minerals are oriented tangentially along the rhizoplane (Figures 4A,D). Some quartz grains are connected to root cells via iron oxides (Figures 2A, 4E). Quartz grains located at the periphery of root cells and close to microbes are frequently surrounded by an organic coating (Figures 2A–C). Amorphous organic matter, reflected by its $^{12}\text{C}^{14}\text{N}$ content (Figure 3), was also identified close to root cells and surrounding mineral particles.

Carbon Transfer at the Root-Rhizosphere Vicinity

Root cell walls are highly enriched in ^{13}C (Figures 3B, 7A–C, 8), with a mean $^{13}\text{C}:^{12}\text{C}$ ratio of 0.024 (SD = 0.004). Within the same section, the $^{13}\text{C}:^{12}\text{C}$ ratio measured in root cell walls varies from

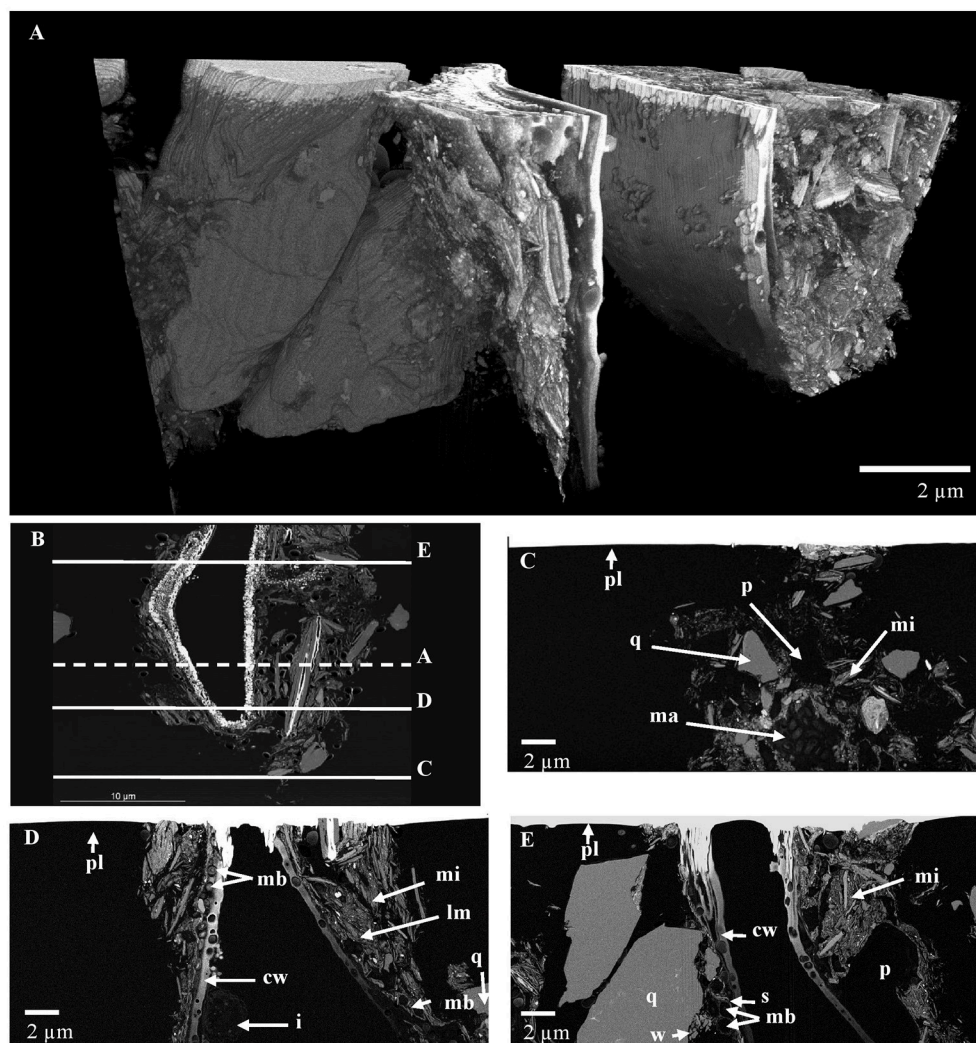


FIGURE 4 | Structural assembly of the intact rhizosphere at a subcellular resolution- FIB-SEM (area indicated in Supplementary Figure 1C). **(A)** Volume visualization of the FIB-SEM dataset representing the interaction between mineral particles and a root cell; **(B)** Virtual perpendicular slice through the FIB-SEM 3D dataset. Letters indicate the position of the selected images; **(C)** Microaggregate at the root periphery; **(D)** Intimate organo-mineral associations; **(E)** Larger mineral particles at the root periphery; cw, cell wall; i, inner cell organic structure; lm, laminar microaggregate; mi, mineral particle; ma, microbial cell assemblage; mb, microorganisms; p, pore; pl, platinum layer; q, quartz grain; s, space between the root cell wall and mineral particles; w, weathering of quartz grain. The overlay of EDS images corresponding to **(C–E)** images are presented in Supplementary Figure 3.

0.018 to 0.032 (**Figure 8**). The enrichment is not homogeneously distributed in the root, as other areas presented a lower $^{13}\text{C}:^{12}\text{C}$ ratio, varying between 0.015 and 0.020 (Supplementary Figure 2).

The mean $^{13}\text{C}:^{12}\text{C}$ ratio of microorganisms is highly variable (0.010–0.029). It is significantly higher than the natural background but lower than the $^{13}\text{C}:^{12}\text{C}$ ratio of plant cell walls, which is 0.016 (SD = 0.004) (**Figures 3B, 7A,B, 8**). The fungal hypha detected in the soil suspension is, on average, slightly ^{13}C enriched (mean $^{13}\text{C}:^{12}\text{C}$ ratio: 0.012), with a significantly higher $^{13}\text{C}:^{12}\text{C}$ ratio compared with the natural background (**Figure 6C**). A highly labeled spot, potentially a hypha-associated microbe, is observed ($^{13}\text{C}:^{12}\text{C}$ ratio: 0.024) (**Figure 6D**). The OC forming a coating around quartz grains is on average not ^{13}C enriched (mean $^{13}\text{C}:^{12}\text{C}$ ratio: 0.011),

with a slight enrichment in a distinct spot ($^{13}\text{C}:^{12}\text{C}$ ratio: 0.015; **Figure 8A**).

DISCUSSION

The Apoplastic Pathway of Carbon at the Root Tip

Some root cell walls are highly enriched in ^{13}C compared with other organic soil compartments (e.g., microorganisms; **Figures 3B, 7, 8**). This illustrates that in the immature root tip, the C transfer is achieved through cell walls, as previously shown at the lab scale by Kaiser et al. (2015). At the root tips, the absence of a Casparian strip enables the flow of recently fixed C (McCully and Canny, 1985) from the stele toward the cortex

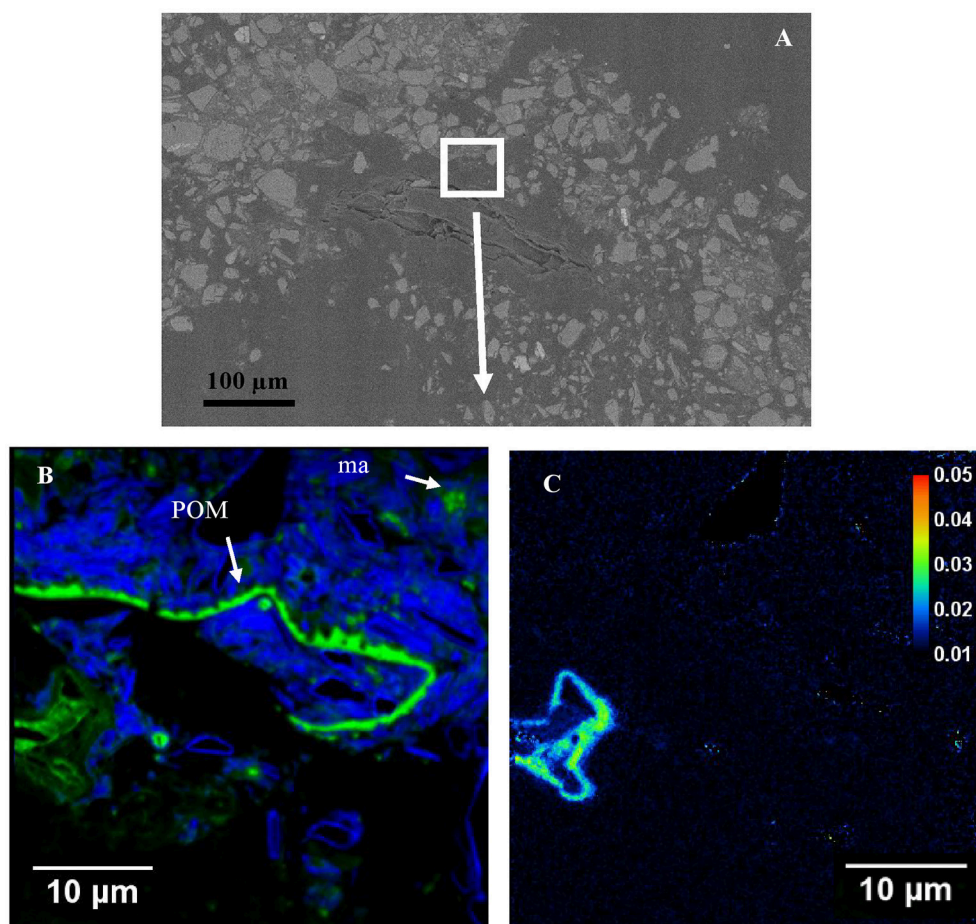


FIGURE 5 | Organo-mineral aggregates surrounding a ^{13}C enriched root cell. **(A)** SEM image of a root surrounded by microaggregates. This image was used to identify areas for subsequent NanoSIMS analyses represented in **(B,C)** images; **(B)** NanoSIMS composite image ($40 \times 40 \mu\text{m}$, 512×512 pixels, 20 planes, $1 \text{ ms} \cdot \text{pixel}^{-1}$); with $^{12}\text{C}^{14}\text{N}$ in green and ^{16}O in blue; POM, particulate organic matter; ma, microbial cell assemblage. **(C)** The $^{13}\text{C}:^{12}\text{C}$ ratio of the same area presented in **(B)**.

via the apoplastic pathway, i.e., along cell walls (Farrar et al., 2003; Jones et al., 2009; Kaiser et al., 2015). The C translocated to the rhizosphere by roots, e.g., root exudates, can be used as substrates by rhizosphere microbial communities (Bertin et al., 2003; Kuzyakov and Blagodatskaya, 2015). In the present study, we focused on root tips described as maximal exudate loss areas along the roots (Jones et al., 2009). It has to be noted that root elongation zones and root hairs are also important locations for root exudation (Rovira, 1973; Sauer et al., 2006).

Active Microbial Communities Close to Root Cells

Microbes surrounding or residing at the rhizoplane were highly enriched in photosynthate-derived ^{13}C (Figures 3B, 7, 8), although lower than root cells. This observation supports our hypothesis that microorganisms surrounding roots incorporated plant-derived C. The lower ^{13}C enrichment observed for microorganisms, compared with root cells reflects a parallel consumption of native soil OC (natural abundance

^{13}C) by microorganisms in the rhizosphere (Kuzyakov and Blagodatskaya, 2015), resulting in the dilution of ^{13}C in bacteria cells. During this process, plant cell walls, which are structural plant components, remained highly ^{13}C enriched (Cotrufo et al., 2015; Vidal et al., 2016). Root-derived C taken up by soil microorganisms is either assimilated, released as metabolites, or respired (Six et al., 2006). Marx et al. (2007) showed in an incubation experiment with root exudates from labeled wheat and maize plants, that more than 50% of the retrieved exudate C was respired as CO_2 by microorganisms. Thus, the lower ^{13}C enrichment observed for microbes may also have resulted from the release of the plant-derived ^{13}C in form of $^{13}\text{CO}_2$ and /or other metabolic products.

The transfer of C to microorganisms is highly dependent on the position of microorganisms in relation to root cells, forming a gradient of foraging on rhizodeposition. As expected, ^{13}C labeled microbes were located at a few micrometers from the root cells (Figures 3B, 7). More distant microbes did not present any enrichment (Figure 5), which is in accordance with

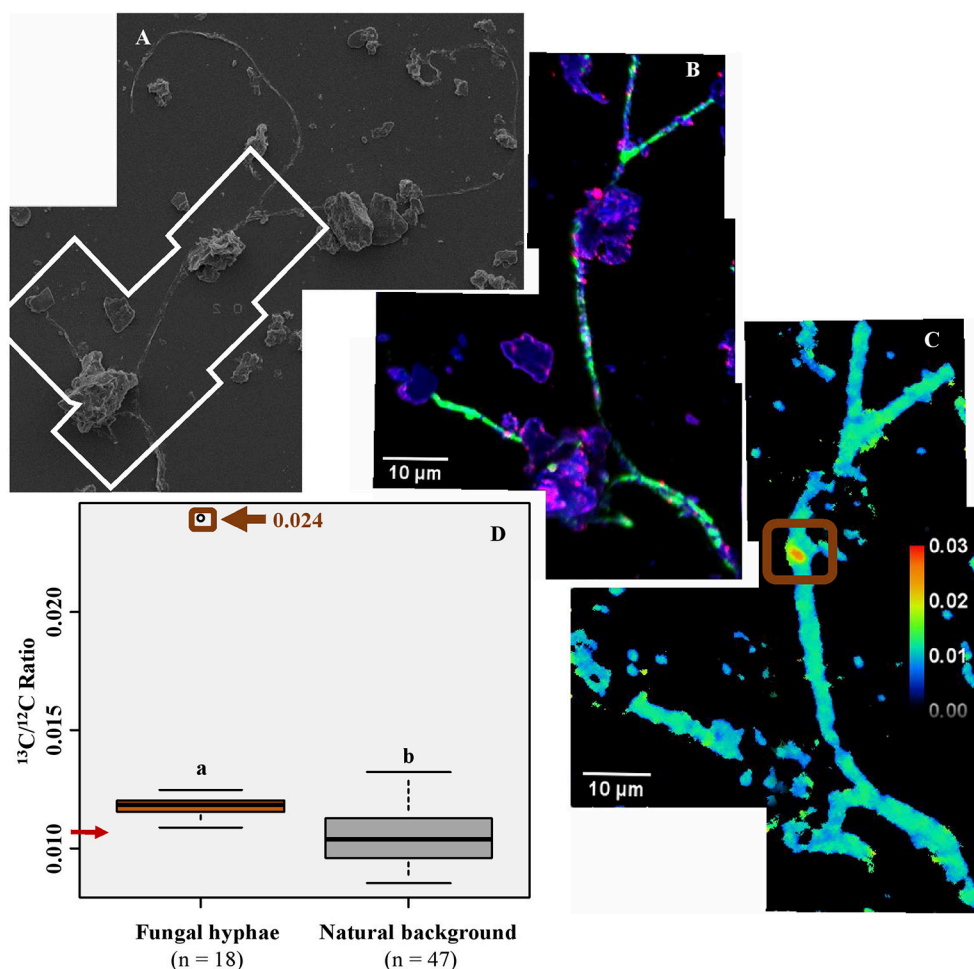


FIGURE 6 | Suspension of soil particles associated with the fungal hypha. The suspension was deposited on a silica wafer, observed with scanning electron microscopy (A) and NanoSIMS (B,C); (B) Mosaic of NanoSIMS composite images; with $^{12}\text{C}^{14}\text{N}$ in green, ^{16}O in blue, $^{56}\text{Fe}^{16}\text{O}$ in red; The mosaic was created from 4 images (one image- $30 \times 30 \mu\text{m}$, 256×256 pixels, 22 planes, $1 \text{ ms} \cdot \text{pixel}^{-1}$); (C) The $^{13}\text{C}:^{12}\text{C}$ ratio of the same area; the brown square indicates a ^{13}C enriched spot on the fungal hyphae. (D) The $^{13}\text{C}:^{12}\text{C}$ ratio for the fungal hypha-Regions of interest (ROIs) was obtained on $^{12}\text{C}^{14}\text{N}$ images, either by using the thresholding function (fungal hypha) or drawing ellipses (natural background); n indicates the number of ROIs drawn. The letters above boxes represent statistical results of Dunn test. The red arrow indicates the $^{13}\text{C}:^{12}\text{C}$ ratio corresponding to natural abundance. The brown square corresponds to the structure highlighted in (C). Boxplots represent the third quartile, the median, the first quartile range of the data, and data outliers.

previous work on microbial communities in the rhizosphere of beech trees (Esperschütz et al., 2009). It has been reported that microbes of the rhizosphere are generally located within a dozen micrometers of the root surface, directly at the rhizoplane or at its close surrounding (Watt et al., 2006a). This distance parameter is directly related to the time of diffusion of a solute from roots to microorganisms (e.g., glucose diffusivity in soil: around $20 \mu\text{m}^2 \cdot \text{s}^{-1}$) (Watt et al., 2006b). This indicates that the closer microbes are to root cells, the higher their chance to receive C-containing substrates.

Fungal Hyphae in the Rhizosphere

The extracted hypha presented a significantly higher $^{13}\text{C}:^{12}\text{C}$ ratio compared with the natural background. This illustrates the role of fungal hyphae as vectors for plant-derived OC into the bulk soil. However, the ^{13}C enrichment was lower compared

with plant cell walls and bacteria cells, with the exception of a ^{13}C enriched spot (Figure 6C). The lower $^{13}\text{C}:^{12}\text{C}$ ratio might result from the ^{13}C dilution process, as described for bacteria cells. It has been shown that most of the plant C allocated to AM fungal hyphae is lost through respiration within 24 h (Johnson et al., 2002; De Deyn et al., 2011). Therefore, the fungal hypha might have been ^{13}C enriched in the past and the ^{13}C enriched signal was probably rapidly diluted by new, non-enriched C coming from the root (De Deyn et al., 2011). We assume that the highly enriched spot represents bacterial cells bound to the fungal hypha. Such strong association of bacterial cells to the hyphal surface was shown before (Artursson et al., 2006; Scheublin et al., 2010; Worrich et al., 2017). As the turnover rate of bacteria is generally considered to be higher compared to fungi (Rousk and Bååth, 2011), the bacteria or group of bacteria might have been transferred to the fungal hypha. It has been shown that bacteria

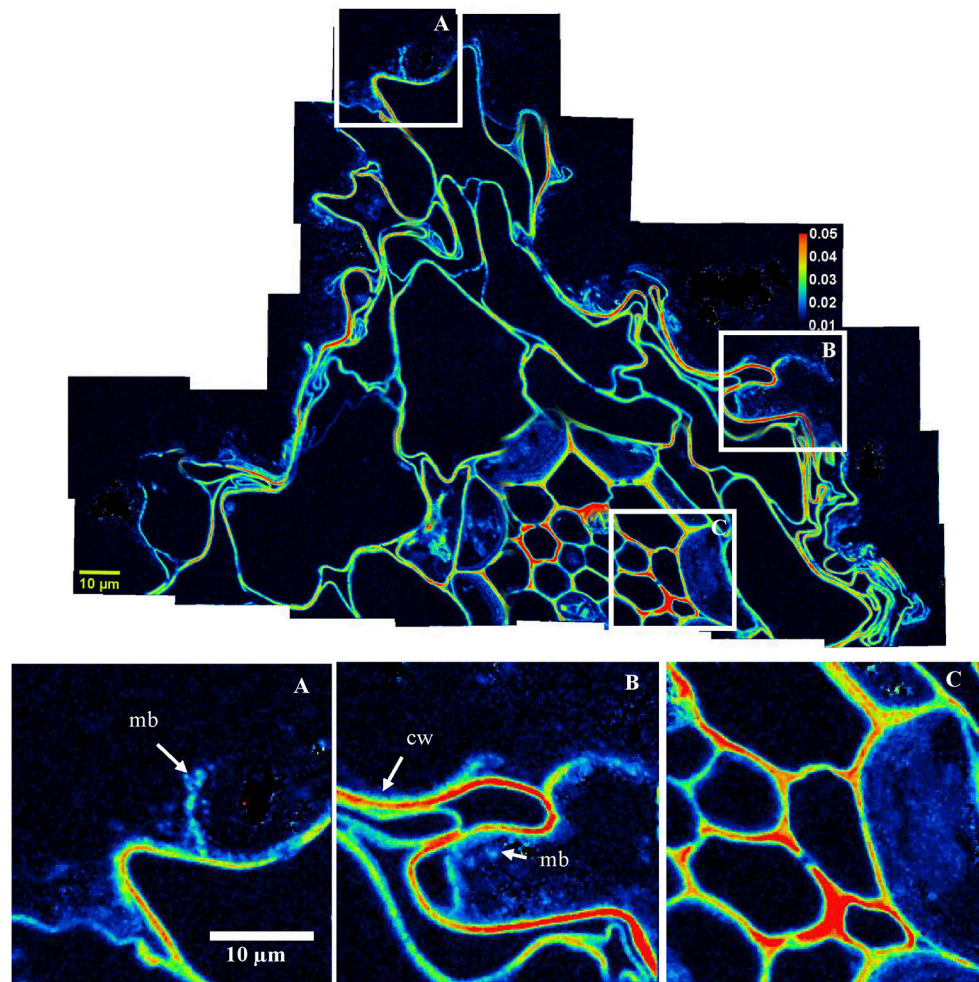


FIGURE 7 | Carbon transfers occurring in the rhizosphere—NanoSIMS images of $^{13}\text{C}:^{12}\text{C}$ ratio of areas highlighted in **Figure 2**. The scale ranges from natural abundance (0.011; dark blue) to highly enriched (0.050; red). The mosaic was created from 32 NanoSIMS images. Three areas (indicated with white squares on the mosaic) are represented below the mosaic for closer observation; **(A,B)**—highlight the transfer of carbon from roots toward the microbial community, intimately associated with the cortex root cells; cw, plant cell walls; mb, microbes. **(C)** Underlines the enrichment of stele cells.

are able to move on fungal hyphae thanks to the production of biofilms (Warmink et al., 2011), the so called “fungal highway.”

The key role of fungal activity in soils is demonstrated by the presence of numerous microaggregates intimately associated with the hyphal surface (**Figure 6B**). We highlight the direct effect of fungal hyphae on the soil microstructure formation, a process which is still poorly understood (Rillig and Mummey, 2006; Lehmann et al., 2017). Mycorrhizal fungi strongly influence soil structure formation through biological (enhancing microbial activity), physical (exerting pressure on the mineral particles), and biochemical (excretion of hyphal products) processes (Chenu, 1989; Rillig and Mummey, 2006; Lehmann et al., 2017). Thus, the mycorrhizal fungal hyphae extend the rhizosphere volume into the root-free bulk soil, acting as a vector for plant-derived OC and fostering soil structure development in root-free bulk soil.

Binding Agents at the Root Surface

The observation of NanoSIMS and FIB-SEM images confirmed our expectations of intimate interactions between mineral particles, microorganisms, and root cells. The deformation of cortex root cells (**Figure 2**) was associated with the tangential orientation of mineral particles along these cells (**Figures 4A,D**). This illustrated the physical compression of soil occurring around roots during the root growth (Foster and Rovira, 1976; Jones et al., 2004). While growing, microorganisms can also exert a pressure on mineral particles at their surroundings, which participate to mediate mineral orientation around microbial aggregates (Foster and Rovira, 1976), as observed in the present study (**Figure 5C**). Thus, the root and microbial growth enhance the intimate association of OC with minerals, probably leading to an increased sorption of OC to mineral surfaces. There is evidence of the association between exudates and soil particles forming a rhizosheath, an

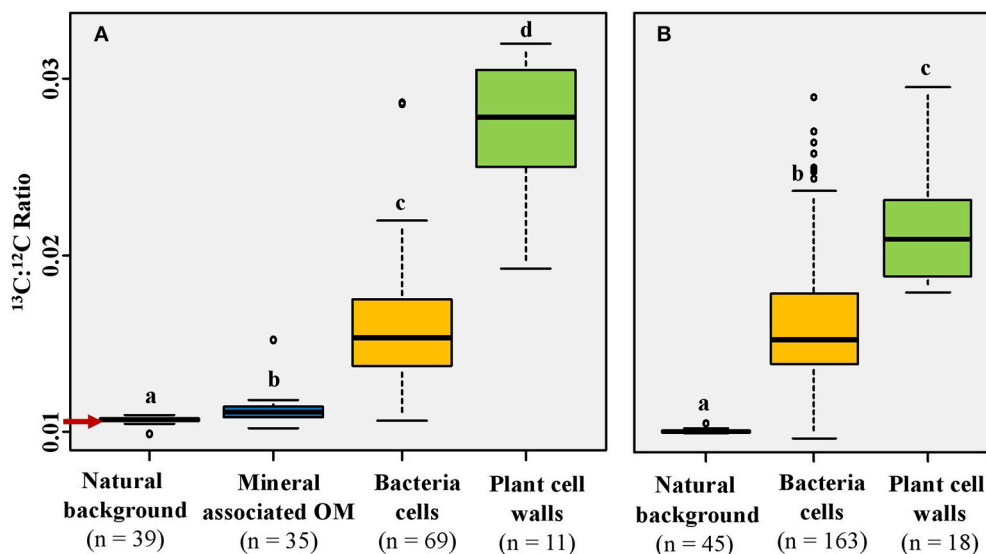


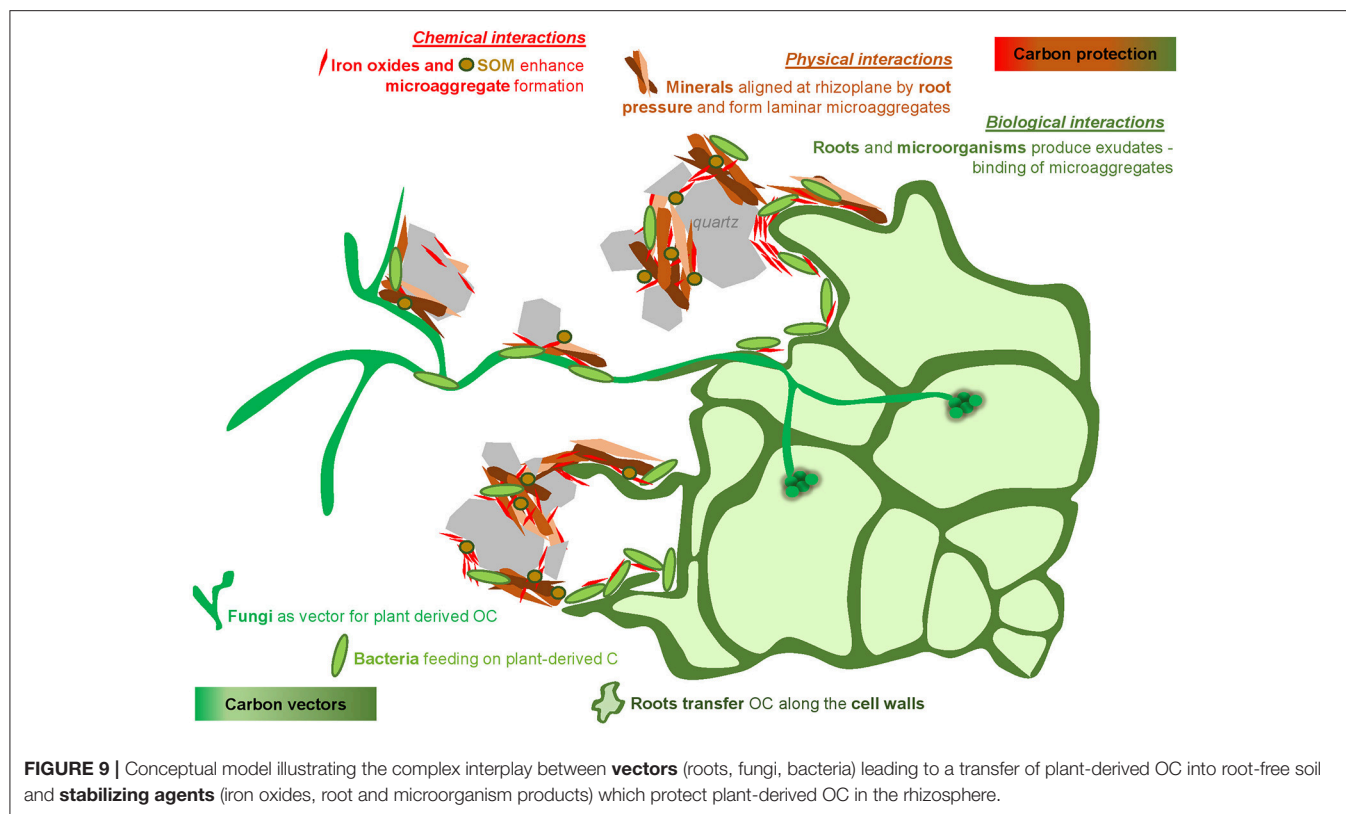
FIGURE 8 | The $^{13}\text{C}:^{12}\text{C}$ ratio distribution according to the type of organic matter. **(A)** $^{13}\text{C}:^{12}\text{C}$ values from areas indicated as white squares in **Figure 2**; **(B)** $^{13}\text{C}:^{12}\text{C}$ values from areas depicted in **Figure 3A**. Regions of interest (ROIs) were obtained on $^{12}\text{C}^{14}\text{N}$ images, either by using the thresholding function (mineral associated OM and bacteria cells), by drawing ellipses (natural background), or by freehand drawing (plant cell walls); n indicates the number of ROIs drawn. The letters above boxes represent statistical results of Dunn test. The red arrow indicates the $^{13}\text{C}:^{12}\text{C}$ ratio corresponding to natural abundance (0.011). Boxplots represent the third quartile, the median, the first quartile range of the data, and data outliers.

aggregated layer around the roots which remains physically stable (Ghezzehei and Albalasmeh, 2015). This process enhances the residence time of OC in the soil, which may contribute to OC sequestration (Rasse et al., 2005; Schmidt et al., 2011).

We assume that the amorphous $^{12}\text{C}^{14}\text{N}$ observed in between the mineral particles close to root cells (**Figure 3**) represents remnants of mucilage, a layer of highly bioavailable C surrounding root tips and acting as a binding agent for soil minerals at the root surface (Jones et al., 2009). This layer can also be seen in the FIB-SEM sections (**Figure 4**), highlighting microbial cells surrounded by a layer of presumably extracellular polymeric substances. Interestingly, most of the microbial cells were found within soil microaggregates, dominated by iron oxides (**Figure 2**). A counteracting process was proposed by Keiluweit et al. (2015) with a dissolution of iron (hydr)oxides and thus release and loss of mineral-associated OM due to the exudation of relatively high amounts of organic acids in artificial rhizospheres. In contrast, our data indicate the presence of iron (hydr)oxides, at natural exudate concentrations, under oxic soil conditions in the vicinity of roots. Oxidizing conditions in the rhizosphere can indeed contribute to the formation of an iron layer made of iron oxidation products, i.e., ferric hydroxide precipitates, at the root surface (Emerson et al., 1999; Kölbl et al., 2017). Ferrous ions, which represent the essential source for iron oxidation, were probably produced in anaerobic microsites created in the rhizosphere (Keiluweit et al., 2016). The large surface area and the high sorption capacity of iron (hydr)oxides, compared with larger particles such as quartz, facilitates the fixation

and protection of microbes within microaggregates (Kögel-Knabner et al., 2008), thus creating a favorable environment for bacteria, which can be found in soil pores not bigger than $1\ \mu\text{m}$ (Watt et al., 2006b), i.e., the typical size of a bacterium.

In the present study, iron oxides were identified as significant binding agents at the root-soil interface by (1) forming bridges between quartz grains and root cells (**Figure 2A**) and (2) being building constituents of organo-mineral microaggregates in the rhizosphere (**Figure 2**). The binding of organic matter to mineral surfaces, including oxides, has been reviewed in the literature (Kögel-Knabner et al., 2008) and more recently directly observed at the microscale (Xiao et al., 2015; Mueller et al., 2017). Iron oxides also represent an essential source of iron for plants and microorganisms in the rhizosphere. Specific mechanisms, such as acidification, reduction, and/or chelation increase iron dissolution and bioavailability in the rhizosphere (Robin et al., 2008). Thus, iron oxides were identified as key components of the rhizosphere, serving as binding agent as well as a potential source of iron for plants and microorganisms. Interestingly, quartz grains, normally described as minor agents for organo-mineral associations, showed patches of organic coatings at their surroundings (**Figures 2A–C**). Those patches had $^{13}\text{C}:^{12}\text{C}$ ratios close to natural abundance with a single spot slightly enriched in ^{13}C (**Figure 8**). Thus, most of the mineral associated OC is represented by native OC rather than derived from the labeled wheat root. This observation supports the idea that most of the C released by the plant is directly transferred to the living microbial community without being directly sorbed to the mineral phase (Kaiser et al., 2015). This indicates a lag phase between the release



of OC by rhizodeposition and the allocation of microbial-derived OC into organo-mineral associated OC in the rhizosphere.

We confirmed that photosynthesis-derived OC was transferred to microorganisms located in the direct root vicinity. As expected, microorganisms, together with soil particles, especially iron oxides, formed microaggregates close to the root surface. We are proposing a conceptual model depicting the fate of carbon at biogeochemical interfaces in the rhizosphere at the forefront of the growing root (**Figure 9**). There is a complex interplay between stabilizing agents which protect plant-derived OC in the rhizosphere, and vectors leading to a transfer of plant-derived OC into root-free soil. Vectors of carbon are represented by (1) **roots**, transferring the carbon through their cell walls, (2) **fungi**, extending the root exploration space, and (3) **microorganisms**, including bacteria, feeding on plant-derived C at the root surface and participating to form a favorable environment for carbon protection in soil microstructures. These **microstructures** arise from the intimate association of organic substances (e.g., bacteria and their exudates, rhizodeposits) and mineral particles (e.g., quartz grains, clay particles, iron (hydr)oxides). **Iron (hydr)oxides** located around roots have a tremendous role in the rhizosphere by closely associating with microorganisms enclosed within microaggregates and by forming bridges with larger mineral particles. Thus, iron oxides can be assumed to have a stabilizing effect on the soil structure in natural rhizospheres. These processes, favoring the transfer and the potential protection of carbon in soil microstructures, are magnified by the physical

pressure exerted by roots, enhancing the close contact of soil minerals and soil organic compartments.

AUTHOR CONTRIBUTIONS

AV collected and analyzed nanoSIMS data, wrote the manuscript, and insured the exchange between all co-authors. JH designed and performed field experimentation and wrote the paper, JH and SFB designed sampling procedures and processed samples, TI processed and analyzed samples, JM and AG supervised the field experiment from which the samples were collected. CH performed nanoSIMS analyses and gave technical support. SS conducted FIB-SEM analyses and output data. CM prepared the samples for nanoSIMS, supervised the analyses, and wrote the manuscript. All authors discussed the results and commented on the manuscript.

FUNDING

Funding by the Swiss National Science Foundation (SNSF), grant No. 406840-143060, as part of the National Research Program NRP68 "Soil as a Resource" is greatly acknowledged. SFB was funded with the latter program [grant no. 143097] and TI was funded by an International short visit grant of the SNSF [grant no. IZK0Z3_164397]. The work was also funded by the Deutsche Forschungsgemeinschaft (DFG), grant No.: MU3021-4/2, as part of the research unit "FOR1806: The Forgotten Part of Carbon Cycling: Organic Matter Storage and Turnover in Subsoils." We

also thank the DFG for funding the nanoSIMS instrument [KO 1035/38-1].

ACKNOWLEDGMENTS

We thank Barbara Orth and Swidran Kanapathipillai for support during field work. Johann Lugmeier is acknowledged for the assistance on the NanoSIMS analyses. We thank Andreas Pfeifer

for giving us the access to the FIB-SEM at the ZEISS Microscopy Customer Center Europe in Oberkochen.

SUPPLEMENTARY MATERIAL

The Supplementary Material for this article can be found online at: <https://www.frontiersin.org/articles/10.3389/fenvs.2018.00009/full#supplementary-material>

REFERENCES

- Abramoff, M. D., Magalhães, P. J., and Ram, S. J. (2004). Image processing with imagej. *Biophoton. Int.* 11, 36–42. Available online at: <https://dx.doi.org/10.1006/bioph.2004.1000>
- Alexander, F. E., and Jackson, R. M. (1954). Examination of soil micro-organisms in their natural environment. *Nature* 174, 750–751. doi: 10.1038/174750b0
- Artursson, V., Finlay, R. D., Jansson, J. K., Artursson, V., Finlay, R. D., and Jansson, J. K. (2006). Interactions between arbuscular mycorrhizal fungi and bacteria and their potential for stimulating plant growth. *Environ. Microbiol.* 8, 1–10. doi: 10.1111/j.1462-2920.2005.00942.x
- Baldock, J., and Skjemstad, J. (2000). Role of the soil matrix and minerals in protecting natural organic materials against biological attack. *Org. Geochem.* 31, 697–710. doi: 10.1016/S0146-6380(00)00049-8
- Bardgett, R. D., Mommer, L., and De Vries, F. T. (2014). Going underground: root traits as drivers of ecosystem processes. *Trends Ecol. Evol.* 29, 692–699. doi: 10.1016/j.tree.2014.10.006
- Bertin, C., Yang, X., and Weston, L. A. (2003). The role of root exudates and allelochemicals in the rhizosphere. *Plant Soil* 256, 67–83. doi: 10.1023/A:1026290508166
- Bronick, C. J., and Lal, R. (2005). Soil structure and management: a review. *Geoderma* 124, 3–22. doi: 10.1016/j.geoderma.2004.03.005
- Castorena, E. V. G., del Carmen Gutiérrez-Castorena, M., Vargas, T. G., Bontemps, L. C., Martínez, J. D., Méndez, E. S., et al. (2016). Micromapping of microbial hotspots and biofilms from different crops using digital image mosaics of soil thin sections. *Geoderma* 279, 11–21. doi: 10.1016/j.geoderma.2016.05.017
- Chenu, C. (1989). Influence of a fungal polysaccharide, scleroglucan, on clay microstructures. *Soil Biol. Biochem.* 21, 299–305. doi: 10.1016/0038-0717(89)90108-9
- Cotrufo, M. F., Soong, J. L., Horton, A. J., Campbell, E. E., Haddix, M. L., Parton, W. J., et al. (2015). Formation of soil organic matter via biochemical and physical pathways of litter mass loss. *Nat. Geosci.* 8, 776–779. doi: 10.1038/ngeo2520
- De Deyn, G., Quirk, H., Oakley, S., Ostle, N., and Bardgett, R. D. (2011). Rapid transfer of photosynthetic carbon through the plant-soil system in differently managed species-rich grasslands. *Biogeosciences* 8, 1131–1139. doi: 10.5194/bg-8-1131-2011
- Dickie, I. A., Martínez-García, L. B., Koele, N., Grelet, G.-A., Tylianakis, J. M., Peltzer, D. A., et al. (2013). Mycorrhizas and mycorrhizal fungal communities throughout ecosystem development. *Plant Soil* 367, 11–39. doi: 10.1007/s11104-013-1609-0
- Emerson, D., Weiss, J. V., and Magonigal, J. P., Emerson, D., Weiss, J. V., and Magonigal, J. P. (1999). Iron-oxidizing bacteria are associated with ferric hydroxide precipitates (Fe-plaque) on the roots of wetland plants. *Appl. Environ. Microbiol.* 65, 2758–2761.
- Esperschütz, J., Buegger, F., Winkler, J. B., Munch, J. C., Schloter, M., and Gatterer, A. (2009). Microbial response to exudates in the rhizosphere of young beech trees (*Fagus sylvatica* L.) after dormancy. *Soil Biol. Biochem.* 41, 1976–1985. doi: 10.1016/j.soilbio.2009.07.002
- Farrar, J., Hawes, M., Jones, D., and Lindow, S. (2003). How roots control the flux of carbon to the rhizosphere. *Ecology* 84, 827–837. doi: 10.1890/0012-9658(2003)084[0827:HRCTFO]2.0.CO;2
- Finzi, A. C., Abramoff, R. Z., Spiller, K. S., Brzostek, E. R., Darby, B. A., Kramer, M. A., et al. (2015). Rhizosphere processes are quantitatively important components of terrestrial carbon and nutrient cycles. *Glob. Chang. Biol.* 21, 2082–2094. doi: 10.1111/gcb.12816
- Flisch, R., Sinaj, S., Charles, R., and Richner, W. (2009). Grundlagen für die düngung im acker- und futterbau. *Agrarforschung* 16, 6–31. Available online at: https://www.agrarforschungschweiz.ch/archiv_11de.php?id_artikel=1449
- Foster, R., and Rovira, A. (1976). Ultrastructure of wheat rhizosphere. *New Phytol.* 76, 343–352. doi: 10.1111/j.1469-8137.1976.tb01469.x
- Ghezzehei, T. A., and Albalasmeh, A. A. (2015). Spatial distribution of rhizodeposits provides built-in water potential gradient in the rhizosphere. *Ecol. Modell.* 298, 53–63. doi: 10.1016/j.ecolmodel.2014.10.028
- Hallett, P. D., Karim, K. H., Glyn Bengough, A., and Otten, W. (2013). Biophysics of the vadose zone: from reality to model systems and back again. *Vadose Zone J.* 12.vzj2013.05.0090. doi: 10.2136/vzj2013.05.0090
- Hinsinger, P., Bengough, A. G., Vetterlein, D., and Young, I. M. (2009). Rhizosphere: biophysics, biogeochemistry and ecological relevance. *Plant Soil* 321, 117–152. doi: 10.1007/s11104-008-9885-9
- Jakobsen, I., and Rosendahl, L. (1990). Carbon flow into soil and external hyphae from roots of mycorrhizal cucumber plants. *New Phytol.* 115, 77–83. doi: 10.1111/j.1469-8137.1990.tb00924.x
- Johnson, D., Leake, J. R., Ostle, N., Ineson, P., and Read, D. J. (2002). *In situ*¹³C₂ pulse-labelling of upland grassland demonstrates a rapid pathway of carbon flux from arbuscular mycorrhizal mycelia to the soil. *New Phytol.* 153, 327–334. doi: 10.1046/j.0028-646X.2001.00316.x
- Jones, D. L., Hodge, A., and Kuzyakov, Y. (2004). Plant and mycorrhizal regulation of rhizodeposition. *New Phytol.* 163, 459–480. doi: 10.1111/j.1469-8137.2004.01130.x
- Jones, D. L., Nguyen, C., and Finlay, R. D. (2009). Carbon flow in the rhizosphere: carbon trading at the soil–root interface. *Plant Soil* 321, 5–33. doi: 10.1007/s11104-009-9925-0
- Kaiser, C., Kilburn, M. R., Clode, P. L., Fuchslueger, L., Koranda, M., Cliff, J. B., et al. (2015). Exploring the transfer of recent plant photosynthates to soil microbes: mycorrhizal pathway vs direct root exudation. *New Phytol.* 205, 1537–1551. doi: 10.1111/nph.13138
- Kallenbach, C. M., Frey, S. D., and Grandy, A. S. (2016). Direct evidence for microbial-derived soil organic matter formation and its ecophysiological controls. *Nat. Commun.* 7:13630. doi: 10.1038/ncomms13630
- Keiluweit, M., Bougoure, J. J., Nico, P. S., Pett-Ridge, J., Weber, P. K., and Kleber, M. (2015). Mineral protection of soil carbon counteracted by root exudates. *Nat. Clim. Chang.* 5, 588–595. doi: 10.1038/nclimate2580
- Keiluweit, M., Nico, P. S., Kleber, M., and Fendorf, S. (2016). Are oxygen limitations under recognized regulators of organic carbon turnover in upland soils? *Biogeochemistry* 127, 157–171. doi: 10.1007/s10533-015-0180-6
- Kögel-Knabner, I., and Amelung, W. (2014). “12.7-Dynamics, chemistry, and preservation of organic matter in soils,” in *Treatise on Geochemistry, 2nd Edn.*, eds K. Turekian and H. Holland (Oxford: Elsevier), 157–215. doi: 10.1016/B978-0-08-095975-7.01012-3
- Kögel-Knabner, I., Guggenberger, G., Kleber, M., Kandeler, E., Kalbitz, K., Scheu, S., et al. (2008). Organo-mineral associations in temperate soils: integrating biology, mineralogy, and organic matter chemistry. *J. Plant Nutr. Soil Sci.* 171, 61–82. doi: 10.1002/jpln.200700048
- Köbl, A., Schweizer, S. A., Mueller, C. W., Höschen, C., Said-Pullicino, D., Romani, M., et al. (2017). Legacy of rice roots as encoded in distinctive microsites of oxides, silicates, and organic matter. *Soils* 1:2. doi: 10.3390/soils1010002
- Kubiena, W. L. (1938). *Micropedology*. Ames, IA: Collegiate Press, Inc.
- Kuzyakov, Y., and Blagodatskaya, E. (2015). Microbial hotspots and hot moments in soil: concept and review. *Soil Biol. Biochem.* 83, 184–199. doi: 10.1016/j.soilbio.2015.01.025
- Kuzyakov, Y., and Domanski, G. (2000). Carbon input by plants into the soil. *Rev. J. Plant Nutr. Soil Sci.* 163, 421–431. doi: 10.1002/1522-2624(200008)163:4<421::AID-JPLN421>3.0.CO;2-R
- Kuzyakov, Y., and Larionova, A. A. (2005). Root and rhizomicrobial respiration: a review of approaches to estimate respiration by autotrophic and

- heterotrophic organisms in soil. *J. Plant Nutr. Soil Sci.* 168, 503–520. doi: 10.1002/jpln.200421703
- Lal, R. (2004). Soil carbon sequestration impacts on global climate change and food security. *Science* 304, 1623–1627. doi: 10.1126/science.1097396
- Lange, M., Eisenhauer, N., Sierra, C. A., Bessler, H., Engels, C., Griffiths, R. I., et al. (2015). Plant diversity increases soil microbial activity and soil carbon storage. *Nat. Commun.* 6:6707. doi: 10.1038/ncomms7707
- Lehmann, A., Zheng, W., and Rillig, M. C. (2017). Soil biota contributions to soil aggregation. *Nat. Ecol. Evol.* 1, 1828–1835. doi: 10.1038/s41559-017-0344-y
- Lehmann, J. (2007). A handful of carbon. *Nature* 447, 143–144. doi: 10.1038/447143a
- Li, Y., Dick, W. A., and Tuovinen, O. H. (2003). Evaluation of fluorochromes for imaging bacteria in soil. *Soil Biol. Biochem.* 35, 737–744. doi: 10.1016/S0038-0717(02)00196-7
- Liang, C., and Balser, T. C. (2011). Microbial production of recalcitrant organic matter in global soils: implications for productivity and climate policy. *Nat. Rev. Microbiol.* 9, 75–75. doi: 10.1038/nrmicro2386-c1
- Martin, J., and Foster, R. (1985). A model system for studying the biochemistry and biology of the root-soil interface. *Soil Biol. Biochem.* 17, 261–269. doi: 10.1016/0038-0717(85)90058-6
- Marx, M., Buegger, F., Gatteringer, A., Zsolnay, Á., and Munch, J. C. (2007). Determination of the fate of ^{13}C labelled maize and wheat exudates in an agricultural soil during a short-term incubation. *Eur. J. Soil Sci.* 58, 1175–1185. doi: 10.1111/j.1365-2389.2007.00911.x
- Mayer, J., Gunst, L., Mäder, P., Samson, M.-F. Carcea, M., Narducci, V., et al. (2015). Productivity, quality and sustainability of winter wheat under long-term conventional and organic management in Switzerland. *Eur. J. Agron.* 65, 27–39. doi: 10.1016/j.eja.2015.01.002
- McCully, M., and Canny, M. (1985). Localisation of translocated ^{14}C in roots and root exudates of field-grown maize. *Physiol. Plant.* 65, 380–392. doi: 10.1111/j.1399-3054.1985.tb08661.x
- Morris, J. K. (1965). A formaldehyde glutaraldehyde fixative of high osmolality for use in electron microscopy. *J. Cell Biol.* 27, 137.
- Mueller, C. W., Hoeschen, C., Steffens, M., et al. (2017). Microscale soil structures foster organic matter stabilization in permafrost soils. *Geoderma* 293, 44–53. doi: 10.1016/j.geoderma.2017.01.028
- Mueller, C. W., Kölbl, A., Hoeschen, C., Hillion, F., Heister, K., Herrmann, A. M., et al. (2012). Submicron scale imaging of soil organic matter dynamics using nanosims - from single particles to intact aggregates. *Org. Geochem.* 42, 1476–1488. doi: 10.1016/j.orggeochem.2011.06.003
- Nunan, N., Ritz, K., Crabb, D., Harris, K., Wu, K., Crawford, J. W., et al. (2001). Quantification of the *in situ* distribution of soil bacteria by large-scale imaging of thin sections of undisturbed soil FEMS Microbiology. *Ecology* 37, 67–77. doi: 10.1111/j.1574-6941.2001.tb00854.x
- Oburger, E., and Schmidt, H. (2016). New methods to unravel rhizosphere processes. *Trends Plant Sci.* 21, 243–255. doi: 10.1016/j.tplants.2015.12.005
- Pett-Ridge, J., and Firestone, M. K. (2017). Using stable isotopes to explore root-microbe-mineral interactions in soil. *Rhizosphere* 3(Pt 2), 244–253. doi: 10.1016/j.rhisph.2017.04.016
- Philippot, L., Raaijmakers, J. M., Lemanceau, P., and van der Putten, W. H. (2013). Going back to the roots: the microbial ecology of the rhizosphere. *Nat. Rev. Microb.* 11, 789–799. doi: 10.1038/nrmicro3109
- Polerecky, L., Adam, B., Milucka, J., Musat, N., Vagner, T., and Kuypers, M. M. (2012). Look@nanosims—a tool for the analysis of nanosims data in environmental microbiology. *Environ. Microbiol.* 14, 1009–1023. doi: 10.1111/j.1462-2920.2011.02681.x
- Ranjard, L., and Richaume, A. (2001). Quantitative and qualitative microscale distribution of bacteria in soil. *Res. Microbiol.* 152, 707–716. doi: 10.1016/S0923-2508(01)01251-7
- Rasse, D. P., Rumpel, C., and Dignac, M.-F. (2005). Is soil carbon mostly root carbon? Mechanisms for a specific stabilisation. *Plant Soil* 269, 341–356. doi: 10.1007/s11104-004-0907-y
- R Core Team (2017). *R: A Language and Environment for Statistical Computing*. Vienna: R Foundation for Statistical Computing. Available online at: www.R-project.org
- Rillig, M. C., and Mummey, D. L. (2006). Mycorrhizas and soil structure. *New Phytol.* 171, 41–53. doi: 10.1111/j.1469-8137.2006.01750.x
- Robin, A., Vansuyt, G., Hinsinger, P., Meyer, J. M., Briat, J. F., and Lemanceau, P. (2008). Iron dynamics in the rhizosphere: consequences for plant health and nutrition. *Adv. Agron.* 99, 183–225. doi: 10.1016/S0065-2113(08)00404-5
- Rousk, J., and Bååth, E. (2011). Growth of saprotrophic fungi and bacteria in soil. *FEMS Microbiol. Ecol.* 78, 17–30. doi: 10.1111/j.1574-6941.2011.01106.x
- Rovira, A. D. (1973). Zones of exudation along plant roots and spatial distribution of micro-organisms in the rhizosphere. *Pest Manag. Sci.* 4, 361–366. doi: 10.1002/ps.2780040313
- Sauer, D., Kuzyakov, Y., and Stahr, K. (2006). Short communication spatial distribution of root exudates of five plant species as assessed by ^{14}C labeling. *J. Plant Nutr. Soil Sci.* 169, 360–362. doi: 10.1002/jpln.200621974
- Scheublin, T. R., Sanders, I. R., Keel, C., van der Meer, J. R., and Scheublin, T. R. (2010). Characterisation of microbial communities colonising the hyphal surfaces of arbuscular mycorrhizal fungi. *ISME J.* 4, 752–763. doi: 10.1038/ismej.2010.5
- Schmidt, M. W., Torn, M. S., Abiven, S., Dittmar, T., Guggenberger, G., Janssens, I. A., et al. (2011). Persistence of soil organic matter as an ecosystem property. *Nature* 478, 49–56. doi: 10.1038/nature10386
- Six, J., Frey, S., Thiet, R., and Batten, K. M. (2006). Bacterial and fungal contributions to carbon sequestration in agroecosystems. *Soil Sci. Soc. Am. J.* 70, 555–569. doi: 10.2136/sssaj2004.0347
- Thévenaz, P., and Unser, M. (2007). User-friendly semiautomated assembly of accurate image mosaics in microscopy. *Microsc. Res. Tech.* 70, 135–146. doi: 10.1002/jemt.20393
- Van der Heijden, M. G., Klironomos, J. N., Ursic, M., Moutoglis, P., Streitwolf-Engel, R., Boller, T., et al. (1998). Mycorrhizal fungal diversity determines plant biodiversity, ecosystem variability and productivity. *Nature* 396, 69–72. doi: 10.1038/23932
- Vidal, A., Remusat, L., Watteau, F., Derenne, S., and Quenea, K. (2016). Incorporation of ^{13}C labelled shoot residues in lumbricus terrestris casts: a combination of transmission electron microscopy and nanoscale secondary ion mass spectrometry. *Soil Biol. Biochem.* 93, 8–16. doi: 10.1016/j.soilbio.2015.10.018
- Wagg, C., Jansa, J., Stadler, M., Schmid, B., and van der Heijden, M. G. (2011). Mycorrhizal fungal identity and diversity relaxes plant-plant competition. *Ecology* 92, 1303–1313. doi: 10.1890/10-1915.1
- Warmink, J. A., Nazir, R., Corten, B., and van Elsland, J. D. (2011). Hitchhikers on the fungal highway: the helper effect for bacterial migration via fungal hyphae. *Soil Biol. Biochem.* 43, 760–765. doi: 10.1016/j.soilbio.2010.12.009
- Watt, M., Hugenholtz, P., White, R., and Vinall, K. (2006a). Numbers and locations of native bacteria on field-grown wheat roots quantified by fluorescence *in situ* hybridization (fish). *Environ. Microbiol.* 8, 871–884. doi: 10.1111/j.1462-2920.2005.00973.x
- Watt, M., Silk, W. K., and Passioura, J. B. (2006b). Rates of root and organism growth, soil conditions, and temporal and spatial development of the rhizosphere. *Ann. Bot.* 97, 839–855. doi: 10.1093/aob/mcl028
- White, P. J., George, T. S., Gregory, P. J., Bengough, A. G., Hallett, P. D., and McKenzie, B. M. (2013). Matching roots to their environment. *Ann. Bot.* 112, 207–222. doi: 10.1093/aob/mct123
- Worrich, A., Stryhanyuk, H., Musat, N., König, S., Banitz, T., Centler, F., et al. (2017). Mycelium-mediated transfer of water and nutrients stimulates bacterial activity in dry and oligotrophic environments. *Nat. Commun.* 8:15472. doi: 10.1038/ncomms15472
- Xiao, J., Wen, Y., Li, H., Hao, J., Shen, Q., Ran, W., et al. (2015). *In situ* visualisation and characterisation of the capacity of highly reactive minerals to preserve soil organic matter (som) in colloids at submicron scale. *Chemosphere* 138, 225–232. doi: 10.1016/j.chemosphere.2015.05.089
- Zadoks, J. C., Chang, T. T., and Konzak, C. F. (1974). A decimal code for the growth stages of cereals. *Weed Res.* 14, 415–421. doi: 10.1111/j.1365-3180.1974.tb01084.x

Conflict of Interest Statement: There are no personal, professional or financial relationships that could potentially be construed as a conflict of interest in the present study.

Copyright © 2018 Vidal, Hirte, Bender, Mayer, Gatteringer, Hoeschen, Schädler, Iqbal and Mueller. This is an open-access article distributed under the terms of the Creative Commons Attribution License (CC BY). The use, distribution or reproduction in other forums is permitted, provided the original author(s) and the copyright owner are credited and that the original publication in this journal is cited, in accordance with accepted academic practice. No use, distribution or reproduction is permitted which does not comply with these terms.